

## Photoneutron cross sections for the silicon isotopes

R. E. Pywell

*Accelerator Laboratory, University of Saskatchewan, Saskatoon, Saskatchewan, Canada S7N 0W0*

B. L. Berman, J. W. Jury,\* and J. G. Woodworth

*Lawrence Livermore National Laboratory, University of California, Livermore, California 94550*

K. G. McNeill

*Department of Physics, University of Toronto, Toronto, Ontario, Canada M5S 1A7*

M. N. Thompson

*School of Physics, University of Melbourne, Parkville, Victoria 3052, Australia*

(Received 15 October 1982)

The photoneutron cross sections for  $^{28}\text{Si}$ ,  $^{29}\text{Si}$ , and  $^{30}\text{Si}$  have been measured up to 33 MeV with monoenergetic photons from the annihilation in flight of fast positrons, using neutron multiplicity counting. Average neutron energies were obtained simultaneously with the cross-section data by the ring-ratio technique. The giant dipole resonances for  $^{28}\text{Si}$  and  $^{30}\text{Si}$  exhibit appreciable fragmentation; that for  $^{29}\text{Si}$  does not. The  $(\gamma, 2n)$  cross section for  $^{30}\text{Si}$  is large; that for  $^{29}\text{Si}$  is consistent with zero. The  $(\gamma, 1n)$  cross section for  $^{30}\text{Si}$  decreases sharply with energy to values near zero as the  $(\gamma, 2n)$  cross section grows, then increases to appreciable values as the  $(\gamma, 2n)$  cross section diminishes; this extreme behavior, although never seen before, is attributable to the competition between the  $(\gamma, n)$ ,  $(\gamma, 2n)$ , and  $(\gamma, pn)$  decay channels. Some properties of the isospin components of the giant resonance are inferred. Other features of the data, including the integrated cross sections, are found to be similar in many respects to corresponding results for the oxygen and magnesium isotopes. The  $^{28}\text{Si}$  nucleus is found to be a better "core" for  $^{29}\text{Si}$  and  $^{30}\text{Si}$  than might have been expected from previous descriptions of its open-shell character.

NUCLEAR REACTIONS  $^{28}\text{Si}(\gamma, n)$ ,  $^{29}\text{Si}(\gamma, n)$ ,  $^{30}\text{Si}(\gamma, n)$ ,  $^{30}\text{Si}(\gamma, 2n)$ ,  
 $E_\gamma = 13.4\text{--}33.1$  MeV; measured  $4\pi$  neutron yields for monoenergetic  
 photons, average photoneutron energies, integrated cross sections; isospin  
 splitting of giant dipole resonance; comparisons of results with oxygen  
 and magnesium isotopes;  $^{28}\text{Si}$  as a "core" nucleus.

### I. INTRODUCTION

The experiments reported in this paper were designed to observe the effects on the giant dipole resonance (GDR) as neutrons are added to a core with closed shells or subshells. It has been observed in the past that the addition of two extra neutrons increases the fragmentation of the GDR, resulting in much structure, for example, for  $^{18}\text{O}$  (Ref. 1) and  $^{26}\text{Mg}$  (Ref. 2). Another feature in light nuclei is the appearance of a pygmy resonance at energies below the GDR as a single extra-core neutron is added, for example, in  $^{13}\text{C}$  (Ref. 3) and  $^{17}\text{O}$  (Ref. 4). One interpretation of the latter feature is that the pygmy resonance is associated with the extra-core neutron, while the GDR is associated with the core and is relatively unchanged by the addition of the valence nu-

cleon. This is the so-called weak-coupling model. [It should be noted, however, that the concept of weak coupling is not nearly so clearly defined for the case of the  $^{15}\text{N}(\gamma, n)$  reaction (Ref. 5), where  $^{15}\text{N}$  is thought of as a proton hole coupled to an  $^{16}\text{O}$  core.] Thus, one can hope to shed light on the concept of  $^{28}\text{Si}$  as a "core" nucleus (closing the  $1d_{5/2}$  subshells in some approximation) by observing the structure and characteristics of the photonuclear cross sections for  $^{28}\text{Si}$ ,  $^{29}\text{Si}$ , and  $^{30}\text{Si}$  both in the pygmy-resonance region and in the GDR proper.

The work reported here was undertaken in conjunction with work performed at the University of Melbourne.<sup>6,7</sup> There the total photoneutron production cross sections for  $^{29}\text{Si}$  and  $^{30}\text{Si}$  were determined by measuring bremsstrahlung yield curves and deriving the cross sections using an unfolding technique.<sup>8,9</sup> Because of the nature of those experiments

TABLE I. Photonuclear thresholds for the silicon isotopes (in MeV).

Nucleus	$E_{\text{thr}}(\gamma, n)$	$E_{\text{thr}}(\gamma, p)$	$E_{\text{thr}}(\gamma, 2n)$	$E_{\text{thr}}(\gamma, pn)$
$^{28}\text{Si}$	17.2	11.6	30.5	24.6
$^{29}\text{Si}$	8.5	12.3	25.7	20.1
$^{30}\text{Si}$	10.6	13.5	19.1	22.9

it was not possible to separate the  $(\gamma, n)$  and  $(\gamma, 2n)$  components of these cross sections. With the higher efficiency detector and the positron-annihilation monoenergetic photons available at Livermore it is possible to separate these components. Therefore the photoneutron cross sections for  $^{29}\text{Si}$  and  $^{30}\text{Si}$  were measured at Livermore in order to complement the high-resolution measurements made at Melbourne in the low-energy region. Threshold energies for photonuclear reactions in the silicon isotopes are given in Table I.

## II. EXPERIMENT

A detailed account of the experimental procedures has been given previously.<sup>1,10</sup> A beam of positrons from the Lawrence Livermore National Laboratory electron-positron linear accelerator is incident on a 0.76-mm thick beryllium annihilation target. Positrons passing through the annihilation target are swept into a well-shielded dump hole. The bremsstrahlung and annihilation photons produced in the target pass through an ionization-chamber beam monitor before striking the photonuclear sample, which is at the center of an efficient  $4\pi$  neutron detector. This detector consists of a 61-cm cube of paraffin in which 48  $\text{BF}_3$  tubes are arranged in four concentric rings around the beam line. Because of the neutron moderation in the paraffin, this arrangement allows a measure to be made of the average neutron energy from the sample via the "ring ratio," the ratio of the counts in the outer and inner rings. A multiplicity analysis of the number of neutrons recorded in each beam burst allows the  $(\gamma, n)$  and  $(\gamma, 2n)$  yields to be extracted simultaneously and independently. The measurements are repeated using electrons so that the bremsstrahlung-induced photoneutrons can be subtracted to give the event rates produced by the annihilation photons alone. For this experiment, the energy of the positrons was varied in approximately 200-keV steps from 17 to 33 MeV. The resolution of the system ranged from about 200 keV (FWHM) at  $E_\gamma = 17$  MeV to about 400 keV at 33 MeV.

For the present work, four samples were required to determine the  $^{28}\text{Si}$ ,  $^{29}\text{Si}$ , and  $^{30}\text{Si}$  cross sections. The characteristics of each sample are given in Table II. The enriched  $^{29}\text{Si}$  and  $^{30}\text{Si}$  samples consist-

ed of  $\text{SiO}_2$  powder contained within thin-walled Lucite cylinders. Since the yield of photoneutrons from the oxygen in these samples makes up a large fraction of the total photoneutron yield, it was necessary to measure the oxygen contribution accurately. In order to avoid the uncertainty resulting from neutron-moderation effects in a water sample, the oxygen yield was determined by subtracting the yield of the Si metal sample from that of the (natural)  $\text{SiO}_2$  sample (after correcting for sample mass, sample size, and photon-absorption effects). This allowed the oxygen contribution for the enriched oxide samples to be determined, thus giving the  $^{29}\text{Si}$  and  $^{30}\text{Si}$  yields. This process resulted in independent measurements being made of the oxygen and natural-silicon cross sections as well as those for  $^{29}\text{Si}$  and  $^{30}\text{Si}$ . The results for  $^{16}\text{O}$  have been reported in a separate paper.<sup>11</sup> The yield from an identical but empty Lucite container also was measured so that the sample-blank photoneutron contribution could be subtracted from all of the above yield data. At each beam energy, measurements were made successively with the  $^{\text{nat}}\text{SiO}_2$ ,  $^{\text{nat}}\text{Si}$ ,  $^{29}\text{SiO}_2$ ,  $^{30}\text{SiO}_2$ , and blank samples using a remote-controlled pneumatic sample-changing device. At intervals throughout each run the measurements were repeated without the annihilation target in place in order to determine the contributions from neutron backgrounds, cosmic rays, and  $\text{BF}_3$  detector noise.

## III. DATA ANALYSIS

A detailed description of the data-reduction procedures has been presented elsewhere.<sup>10</sup> Therefore, only a brief account of those features relevant to the present experiment will be given here.

TABLE II. Sample specifications.

Sample	Mass (g)	Relative abundance (at. %)		
		$^{28}\text{Si}$	$^{29}\text{Si}$	$^{30}\text{Si}$
$^{\text{nat}}\text{Si}$	51.3	92.23	4.67	3.10
$^{\text{nat}}\text{SiO}_2$	97.3	92.23	4.67	3.10
$^{29}\text{SiO}_2$	82.4	4.36	95.28	0.36
$^{30}\text{SiO}_2$	78.9	3.78	0.67	95.55

After a small (never more than a few percent) correction for the pileup of counts in the neutron detector, the annihilation-target-out background runs were subtracted from the positron and electron yield measurements. Then at each energy, normalized neutron yields for the runs using electrons were subtracted from the corresponding yields obtained with positrons. This was done for all four samples and for the sample blank. Finally, the appropriately normalized sample-blank yields were subtracted to give the  $^{nat}\text{SiO}_2$ ,  $^{nat}\text{Si}$ ,  $^{29}\text{SiO}_2$ , and  $^{30}\text{SiO}_2$  yields.

Then, as indicated in the previous section and in more detail in Ref. 11, the  $^{nat}\text{Si}$  metal-sample yields were normalized to those for  $^{nat}\text{SiO}_2$ . The yield resulting from the oxygen alone then was determined by subtraction. These yields are shown in Fig. 1 of Ref. 11. This oxygen yield was in turn normalized to the  $^{29}\text{SiO}_2$  and  $^{30}\text{SiO}_2$  yields, as shown here in Fig. 1, and subtracted to obtain the yields resulting from

only the silicon isotopes in each sample. The systematic uncertainty resulting from the oxygen normalization is less than 2%. This procedure is not necessary for the double-neutron yields, because the  $(\gamma, 2n)$  cross section for  $^{16}\text{O}$  is very small in this energy range (see Refs. 12 and 13) and the resulting double-neutron yield from oxygen was insignificant.

From the net yield rates the photoneutron cross sections for each sample were obtained. This procedure involves (a) a correction for the neutron multiplicity in order to ascertain the true number of single- and double-photoneutron events, (b) a correction for the detector efficiency for each energy point using the measured ring ratio (see Refs. 14–16), (c) a correction for the (atomic) attenuation of photons in the sample, and finally (d) the conversion into cross-section units using the calibrated ion-chamber response per annihilation photon and the number of sample nuclei in the beam.

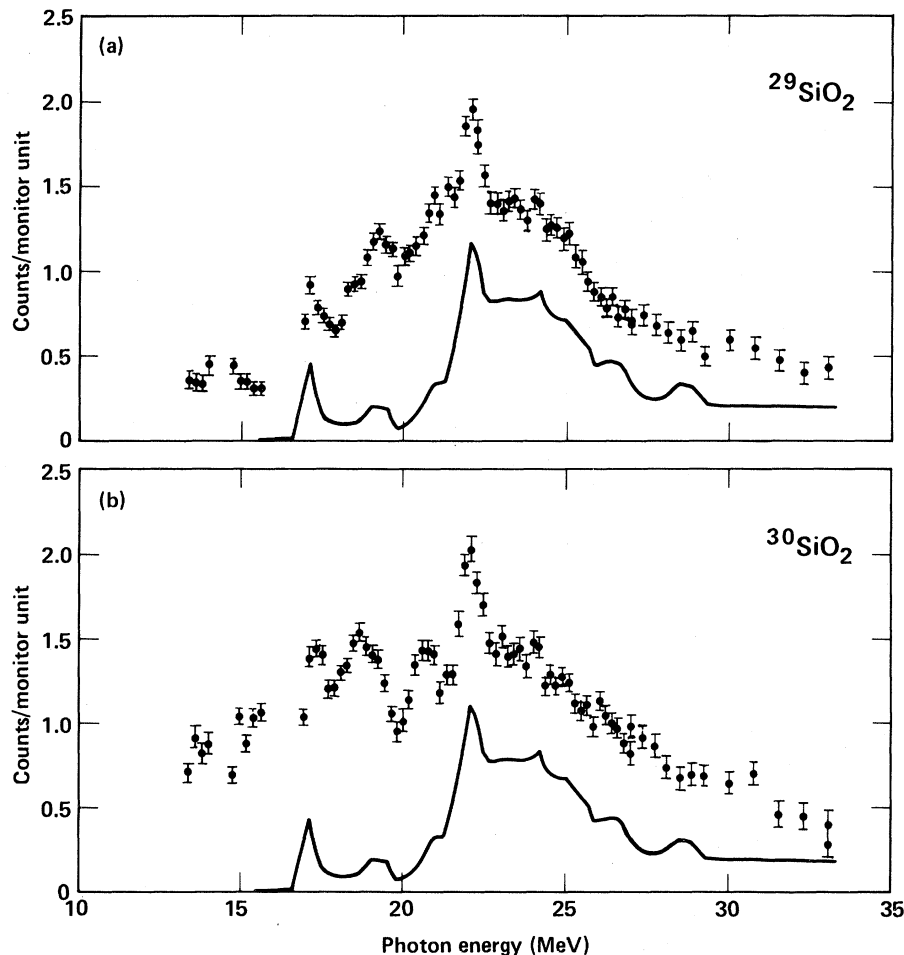


FIG. 1. Net single-photoneutron yield rates for the samples of (a)  $^{29}\text{SiO}_2$  and (b)  $^{30}\text{SiO}_2$ , together with the corresponding normalized yield rate for  $\text{O}_2$  for each case, thus showing the magnitude of the necessary oxygen subtractions.

Since no sample was isotopically pure, the cross sections for each isotope ( $^{28}\text{Si}$ ,  $^{29}\text{Si}$ , and  $^{30}\text{Si}$ ) were then extracted from the measured cross sections using the known isotopic compositions, given in Table II, and using the fact that the cross section for each sample was a weighted sum of the contributions from each isotope.

As discussed in detail in Refs. 1 and 10, the overall absolute systematic uncertainty in the total photoneutron cross sections increases from about 7% at the lower photon energies to about 10–12% at the highest energy measured here.

#### IV. RESULTS AND DISCUSSION

##### A. $^{\text{nat}}\text{Si}$

The present photoneutron cross-section results for  $^{\text{nat}}\text{Si}$  were obtained directly from the metallic silicon sample, and are presented (as the data points) in both parts of Fig. 2. The single-photoneutron cross section  $\sigma(\gamma, 1n)$  [note that this cross section includes the  $(\gamma, pn)$  channel] rises from the  $^{28}\text{Si}(\gamma, n)$  threshold at 17.2 MeV to several prominent intermediate-structure peaks between about 18 and 22 MeV and then falls off very gradually from 22 to 33 MeV.

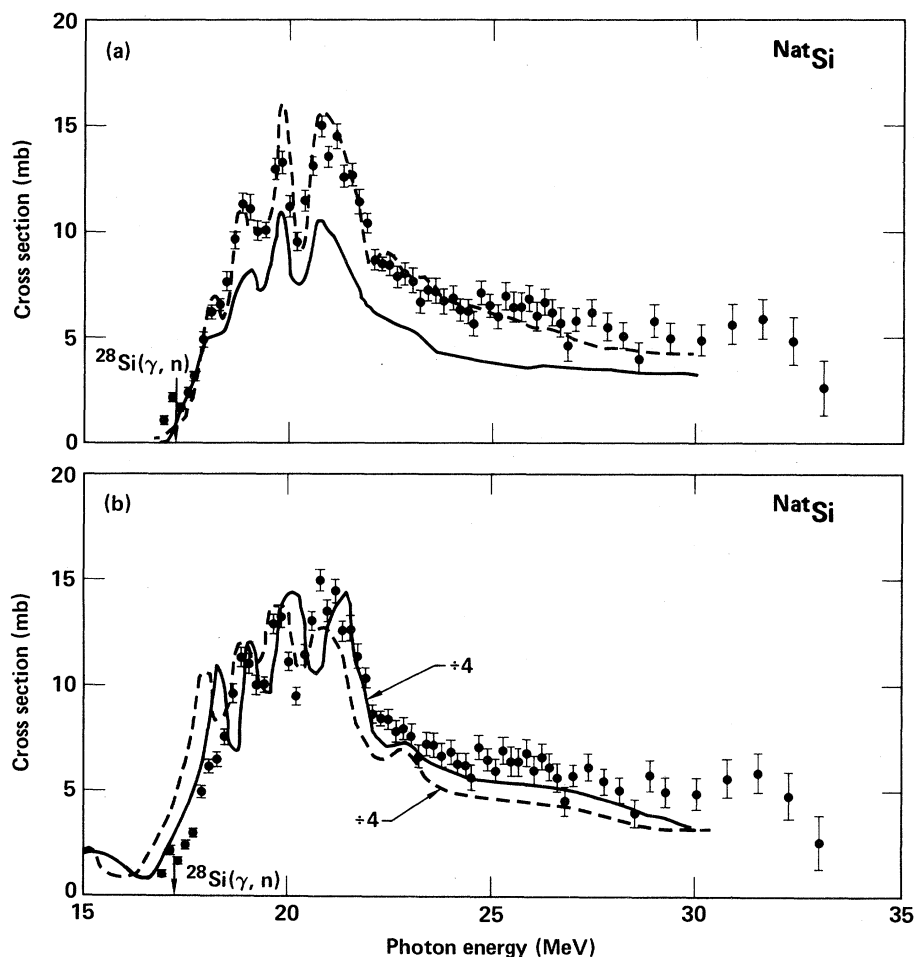


FIG. 2. Present results for  $\sigma(\gamma, 1n)$  for  $^{\text{nat}}\text{Si}$  (data points) compared with previous results: (a)  $\sigma(\gamma, 1n)$  from Livermore (Ref. 17, solid line) and from Saclay (Ref. 12, dashed line); (b)  $\sigma(\gamma, \text{tot})$  from Ljubljana (Ref. 22, dashed line) and from Mainz (Ref. 23, solid line). The arrows here and in subsequent figures indicate photoneutron reaction thresholds (see Table I). The error flags here and in subsequent figures represent the statistical uncertainties (only) for the cross sections obtained in the present experiment.

No statistically significant  $(\gamma, 2n)$  events were observed.

Figure 2(a) compares the present  $^{nat}\text{Si}(\gamma, 1n)$  cross-section results with previous results obtained with monoenergetic photons at Livermore<sup>17</sup> (solid line) and Saclay<sup>12</sup> (dashed line). In the GDR region (up to  $\sim 23$  MeV) the present results are intermediate in magnitude between those of Refs. 12 and 17, but are rather closer to the Saclay results than to these very early Livermore values. Near 25 MeV the present results are approximately equal to the Saclay values, and above  $\sim 27$  MeV the present results exceed both previous results although there is no im-

portant disagreement with the Saclay values above 22 MeV. Thus the present measurement resolves a large and long-standing discrepancy between the results of Refs. 12 and 17. We note as well that the present results agree, on the whole, quite well with the earlier results of Refs. 18–20 obtained with bremsstrahlung photons.

There also have been several total photon absorption measurements on  $^{nat}\text{Si}$  (Refs. 21–23), from which the total photonuclear cross section  $\sigma(\gamma, \text{tot})$  has been obtained. Results of this kind, obtained at Ljubljana<sup>22</sup> and at Mainz,<sup>23</sup> are compared in Fig. 2(b) with the  $(\gamma, 1n)$  cross section. Since  $\sigma(\gamma, \text{tot})$  in-

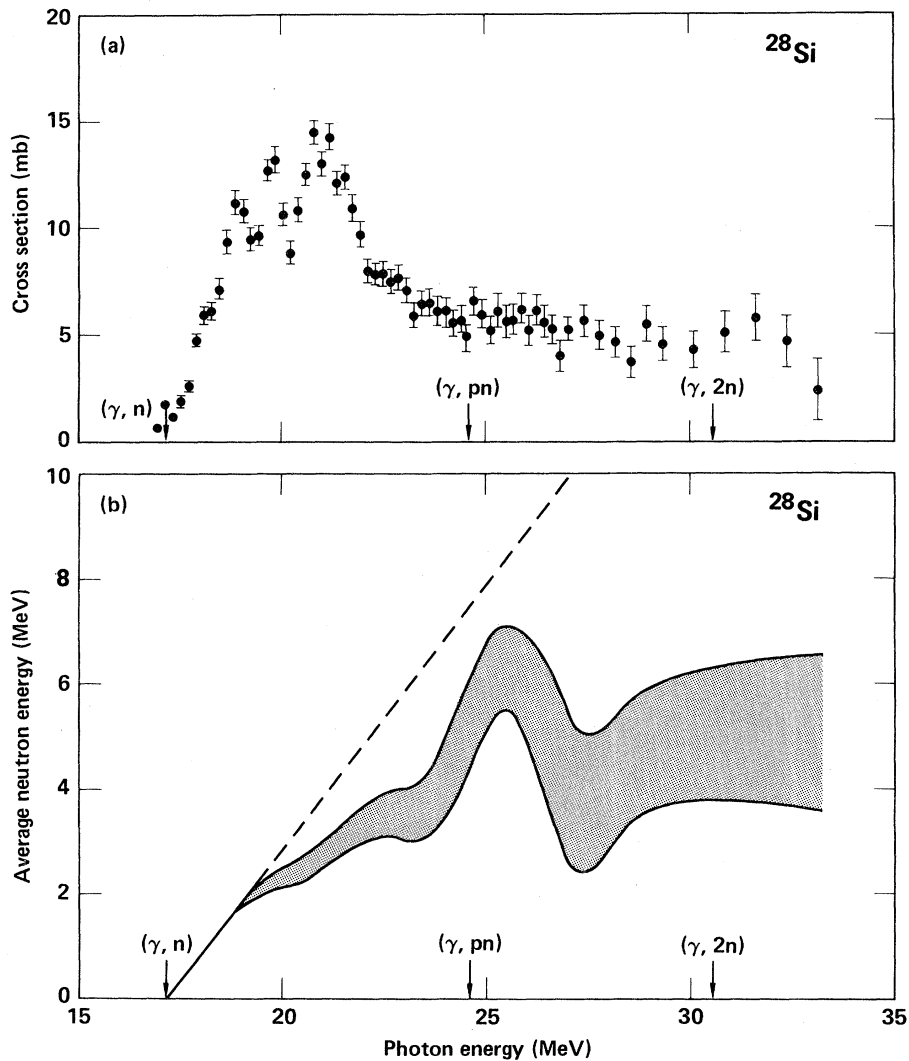


FIG. 3. Present results for  $^{28}\text{Si}$ : (a) single-photon-neutron cross section  $\sigma(\gamma, 1n)$ ; (b) average single-photon-neutron energy  $\bar{E}_n(\gamma, 1n)$ .

cludes  $\sigma(\gamma,p)$  as well as  $\sigma(\gamma,n)$ , and since  $\sigma(\gamma,p)$  is several times the magnitude of  $\sigma(\gamma,n)$  (see Ref. 24, for example), it is notable that the overall shape of  $\sigma(\gamma,\text{tot})$  is very similar to that of  $\sigma(\gamma,1n)$ , as is seen in Fig. 2(b). The most obvious exception to this is the peak at  $\sim 18$  MeV, which is relatively much more prominent in  $\sigma(\gamma,\text{tot})$  than in  $\sigma(\gamma,1n)$ ; but this can be ascribed to the fact that the  $^{28}\text{Si}(\gamma,p)$  threshold is much lower than the  $(\gamma,n)$  threshold (see Table I), and that the 18-MeV peak is only  $\sim 0.8$  MeV above the  $(\gamma,n)$  threshold, so that there are many more states in the residual nucleus accessible to the  $(\gamma,p)$  channel than to the  $(\gamma,n)$  channel (the first excited state of  $^{27}\text{Si}$  is at 0.78 MeV). The earlier  $\sigma(\gamma,\text{tot})$  results from National Bureau of Standards<sup>21</sup> (NBS) exhibit much the same shape as those of Refs. 22 and 23, albeit with poorer statistics. Possibly more important, however, is the fact that the absolute magnitude of  $\sigma(\gamma,\text{tot})$  from Ref. 21 is lower by more than 20% than that from Ref. 23. This is important partly because the difference between  $\sigma(\gamma,\text{tot})$  and  $\sigma(\gamma,n)$  implies a value for  $\sigma(\gamma,p)$  and consequently for the ratio  $\sigma(\gamma,p)/\sigma(\gamma,n)$ , which in turn is important for isospin considerations (see Secs. IV C and IV D).

It is clear from high-resolution measurements of  $\sigma(\gamma,n_0)$  (Ref. 25) and  $\sigma(\gamma,p_0)$  (Ref. 26) that the peaks seen here represent intermediate structure, and are made up of many fine-structure resonances.

#### B. Cross sections and average neutron energies for the silicon isotopes

As noted above, the data for the enriched samples of  $^{28}\text{Si}$ ,  $^{29}\text{Si}$ , and  $^{30}\text{Si}$  were corrected for their mutual contamination so that the results for each silicon isotope could be extracted as if the samples were 100% pure. Since the samples were indeed nearly 100% pure (see Table II), this correction introduced negligible additional uncertainty.

##### 1. $^{28}\text{Si}$

Figure 3(a) shows the results for  $\sigma(\gamma,1n)$  for  $^{28}\text{Si}$ . The main part of the GDR for this nucleus is centered at  $\sim 21$  MeV. Peaks or shoulders in the cross section are observed at 18.1, 18.9, 19.8, 20.8, 21.2, 22.4, and possibly 23.5 MeV, in excellent agreement with the results of Refs. 12 and 17. The average photoneutron energy  $\bar{E}_n$ , shown in Fig. 3(b), rises from threshold to a maximum of  $\sim 7$  MeV near  $E_\gamma \gtrsim 25$  MeV, followed by a relative minimum of  $\sim 3$  MeV at  $E_\gamma \lesssim 28$  MeV. This decrease of  $\bar{E}_n$  probably can be attributed to the opening of the  $(\gamma,pn)$  reaction channel at 24.6 MeV.

##### 2. $^{29}\text{Si}$

Figure 4(a) shows the results for  $\sigma(\gamma,1n)$  for  $^{29}\text{Si}$ . The main part of the GDR for this nucleus is centered at  $\sim 20$  MeV and is relatively featureless, as has been noted in the past for odd- $A$  isotopes in a sequence  $[(4N+1)$  nuclei] in the  $s$ - $d$  shell, as for  $^{17}\text{O}$  (Ref. 4) and for  $^{25}\text{Mg}$  (Ref. 27). Although they are not very well-defined, peaks or shoulders in the cross section can be discerned at about 17.5, 19.3, 21.2, 21.9, and 24.6 MeV, as well as a broad hump centered near 30 MeV. Again, such peaks as are seen here are very likely of intermediate-structure nature, as evidenced by the large amount of fine structure found in the  $(\gamma,p_0)$  reaction channel for  $^{29}\text{P}$  (Ref. 28). Up to 25 MeV, the recent data obtained with bremsstrahlung photons at Melbourne (Ref. 6) are in good agreement with the present results, with regard both to absolute magnitude and to shape. Below 17 MeV, the high-resolution data of Ref. 6 are much more detailed than the present data in this energy region. From 25 to 28 MeV, the cross section reported in Ref. 6 makes a sizable upward excursion which is greater than that in the present data. This discrepancy probably can be attributed to the well-known difficulty of extracting cross-section information above the GDR by means of a bremsstrahlung-unfolding technique. The high-energy strength seen in the present data cannot result from the  $(\gamma,2n)$  reaction channel because the absence of statistically significant  $(\gamma,2n)$  events in the present data enables us to set an upper limit of  $\sim 0.2$  mb on  $\sigma(\gamma,2n)$  for  $^{29}\text{Si}$  even at the highest energy measured here.

The average photoneutron energy for  $^{29}\text{Si}$  is shown in Fig. 4(b). It is seen that  $\bar{E}_n$  rises rapidly at low energies, so that one can infer that the  $(\gamma,n)$  cross section is consistent with 100% ground-state transitions up to at least 15 MeV (see the discussion of isospin in Sec. IV D). A sharp drop in  $\bar{E}_n$  above 17 MeV indicates the onset of the GDR proper for this nucleus, and  $\bar{E}_n$  is relatively low for the entire energy region from 18 to 26 MeV, implying a high degree of collectivity of the GDR for this nucleus. The further decrease in  $\bar{E}_n$  just above 22 MeV probably results from branching into the  $(\gamma,pn)$  channel. The sharp rise above 27 MeV, since it cannot arise from the  $(\gamma,2n)$  channel, indicates that a major fraction of the decay at these energies above the GDR proper must populate the ground state or other low-lying states in  $^{28}\text{Si}$ , and thus may signify the onset of additional  $T_<$  strength there (defined and discussed in Sec. IV C), as has been seen previously in the lighter  $4N \pm 1$  nuclei  $^{13}\text{C}$ ,  $^{15}\text{N}$ , and  $^{17}\text{O}$  (Refs. 3, 5, and 4, respectively).

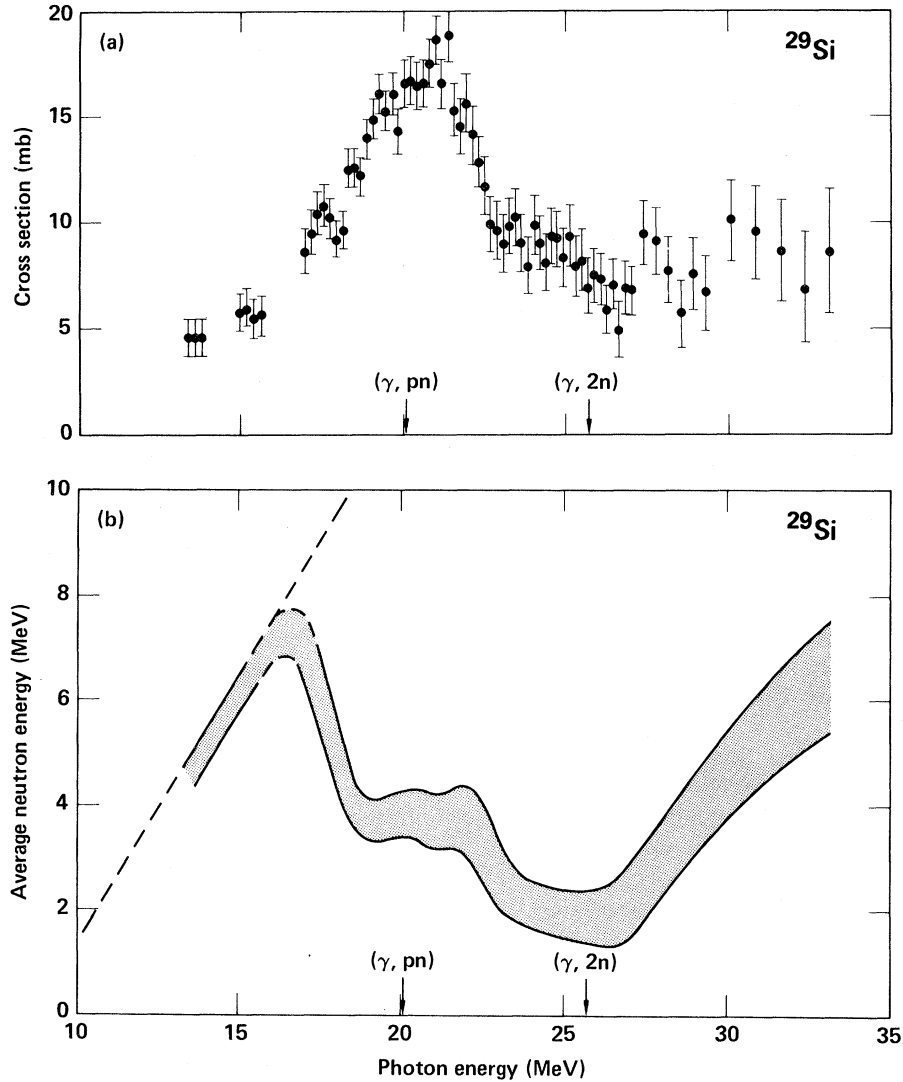


FIG. 4. Present results for  $^{29}\text{Si}$ : (a) single-photon neutron cross section  $\sigma(\gamma, 1n)$ ; (b) average single-photon neutron energy  $\bar{E}_n(\gamma, 1n)$ .

### 3. $^{30}\text{Si}$

The single-photon neutron cross section  $\sigma(\gamma, 1n)$  for  $^{30}\text{Si}$  is shown in Fig. 5(a). The most striking feature of this cross section is its sharp decrease from just above its maximum of  $\sim 20$  mb at 18.7 MeV to very low values, not much greater than zero, in the photon-energy region from 23 to 25 MeV, followed by a rise to values near 7 mb by  $\sim 27$  MeV. This extreme behavior could not have been predicted from

previous studies of the  $(4N+2)$  nuclei in the  $s$ - $d$  shell,  $^{18}\text{O}$  (Ref. 1) and  $^{26}\text{Mg}$  (Ref. 2), although the depletion of the  $(\gamma, n)$  channel in favor of the  $(\gamma, 2n)$  reaction channel by a few MeV above the  $(\gamma, 2n)$  threshold is common for medium and heavy nuclei (see Ref. 29, for example).

The results for  $\bar{E}_n$  vs  $E_\gamma$  for the  $(\gamma, 1n)$  reaction in  $^{30}\text{Si}$  are shown in Fig. 5(b). Here again the data are striking, especially the narrow ( $\sim 1$  MeV wide) spike in  $\bar{E}_n$  (up to  $\sim 8$  MeV) centered at  $E_\gamma = 19.5$  MeV, which shows the existence of strong ground-state

transitions near that energy, in the middle of the GDR. The decrease of  $\bar{E}_n$  above 25 MeV, together with the rise of  $\sigma(\gamma, 1n)$  above that energy, implies strongly that the  $(\gamma, 1n)$  cross section is dominated by the  $(\gamma, pn)$  channel above  $\sim 26$  MeV.

The above assertion is reinforced by the behavior of the  $(\gamma, 2n)$  cross section, shown in Fig. 6(a). Unlike the behavior of  $\sigma(\gamma, 2n)$  for  $^{18}\text{O}$  and  $^{26}\text{Mg}$  (Refs. 1 and 2), it falls steadily from its maximum value of  $\sim 9$  mb at 22–24 MeV to quite low values at the higher energies measured (2–3 mb at 29–31 MeV). Thus one observes the sequential passing of strength from the  $(\gamma, n)$  to the  $(\gamma, 2n)$  to the  $(\gamma, pn)$  channels,

which implies a statistical behavior not necessarily expected to hold in a nucleus as light as  $^{30}\text{Si}$ . The gradual rise of  $\bar{E}_n$  for the  $(\gamma, 2n)$  reaction channel for  $^{30}\text{Si}$  is shown in Fig. 6(b).

Figure 7 shows the combined photoneutron data for  $^{30}\text{Si}$ : part (a) shows the total photoneutron cross section

$$\sigma(\gamma, n_{\text{tot}}) = \sigma[(\gamma, 1n) + (\gamma, 2n)]$$

and part (b) shows  $\sigma(\gamma, 1n)$  and  $\sigma(\gamma, 2n)$  superposed and plotted on the same scale. The data in Fig. 7(b) are presented here to make clear the relationship

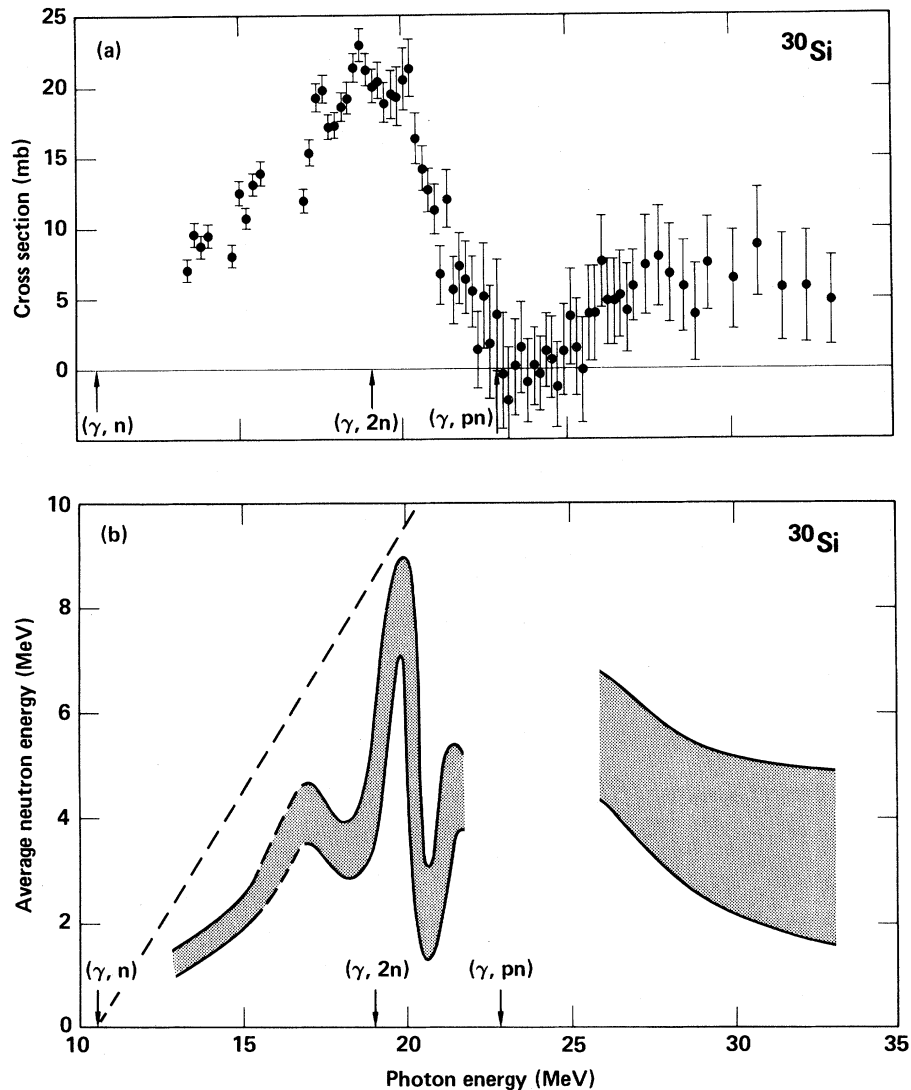


FIG. 5. Present single-photoneutron results for  $^{30}\text{Si}$ : (a)  $\sigma(\gamma, 1n)$ ; (b)  $\bar{E}_n(\gamma, 1n)$ . In the region from about 22 to 26 MeV, the near-zero cross section precludes an accurate determination of  $\bar{E}_n$ .

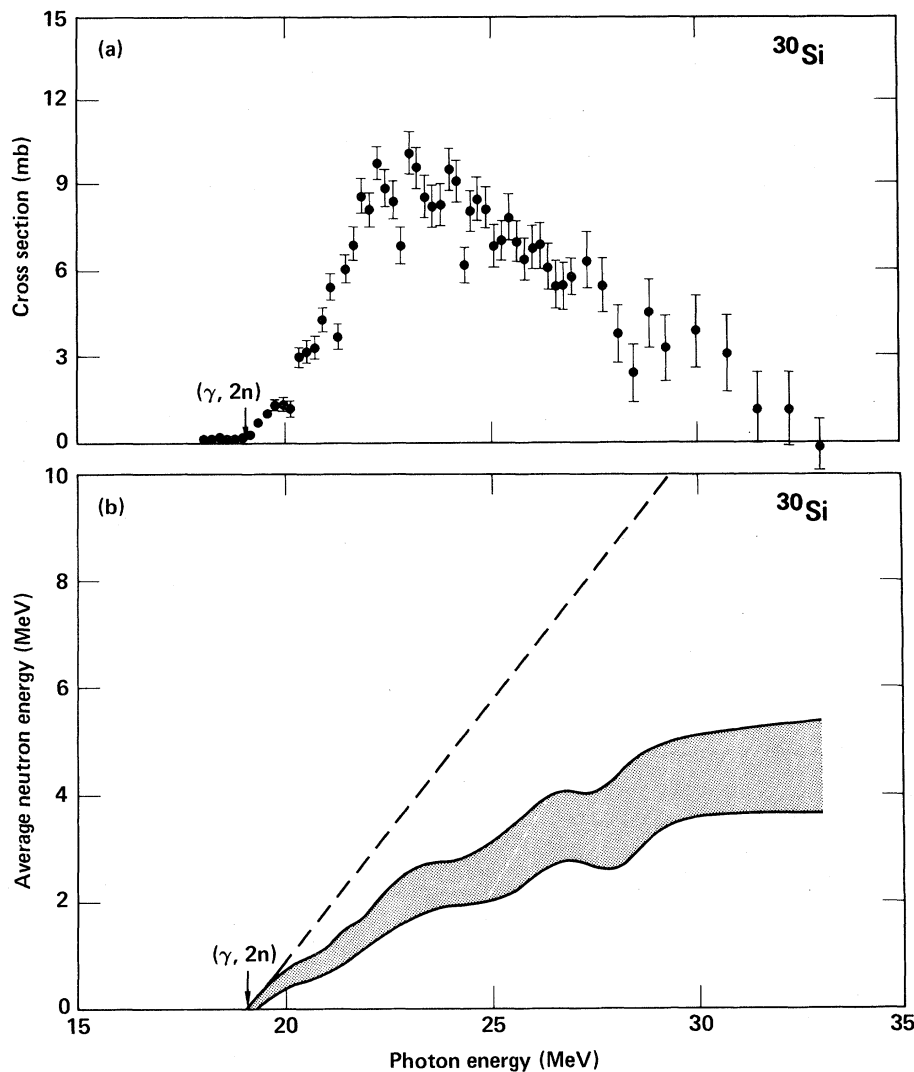


FIG. 6. Present double-photon neutron results for  $^{30}\text{Si}$ : (a)  $\sigma(\gamma, 2n)$ ; (b)  $\bar{E}_n(\gamma, 2n)$ .

among the various photoneutron reaction channels discussed above. The main part of the GDR, as seen in the  $(\gamma, n_{\text{tot}})$  cross section [Fig. 7(a)], is centered at  $\sim 19$  MeV. Evidence for peaks in  $\sigma(\gamma, n_{\text{tot}})$  can be seen at 17.5, 18.6, and 20.3 MeV.

#### 4. Comparison of $^{28}\text{Si}$ , $^{29}\text{Si}$ , and $^{30}\text{Si}$

Figure 8 compares the data for  $\sigma(\gamma, n_{\text{tot}})$  for  $^{28}\text{Si}$  [part (a)],  $^{29}\text{Si}$  [part (b)], and  $^{30}\text{Si}$  [part (c)], all plotted to the same scale. Also included in parts (b) and (c) are the bremsstrahlung data up to the  $(\gamma, 2n)$  thresholds from Melbourne for  $^{29}\text{Si}$  (Ref. 6) and for  $^{30}\text{Si}$  (Ref. 7); these data are in reasonable agreement with the overlap data obtained in the present measurement. It is clear from Fig. 8 that

$\sigma(\gamma, n_{\text{tot}})$  increases greatly as neutrons are added to the  $^{28}\text{Si}$  core, very likely indicating that a rapidly increasing fraction of the dipole strength (at least below 33 MeV) appears in the neutron decay channels.

#### C. Isospin considerations

The photoneutron cross sections for all three silicon isotopes presented in this paper allow some comment to be made on the systematic effects of isospin. Unfortunately, the amount of information that can be deduced here is limited by the fact that detailed measurements of the photoproton decay channel for  $^{29}\text{Si}$  and  $^{30}\text{Si}$  are not yet available.<sup>30</sup>

Dipole photon absorption by a nucleus of ground-state isospin

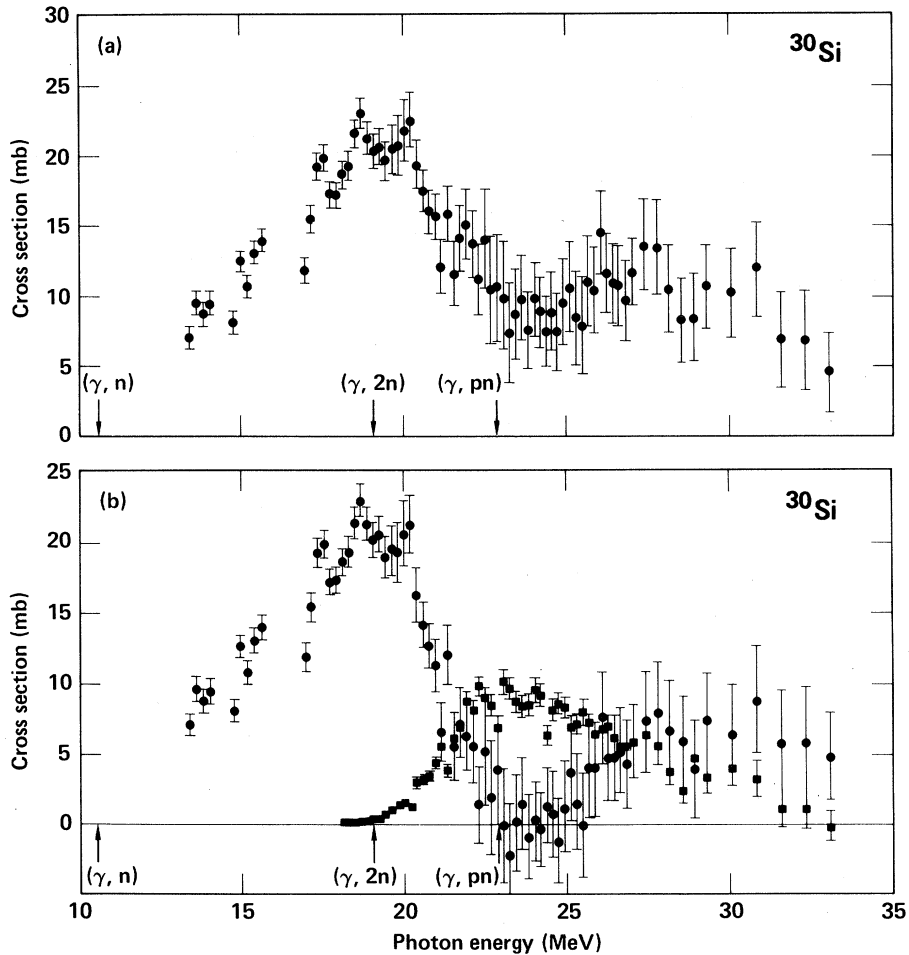


FIG. 7. Present cross-section results for  $^{30}\text{Si}$ : (a) total photoneutron cross section  $\sigma(\gamma, n_{\text{tot}}) = \sigma(\gamma, 1n) + \sigma(\gamma, 2n)$ ; (b)  $\sigma(\gamma, 1n)$  (round data points) and  $\sigma(\gamma, 2n)$  (square data points).

$$T_0 = (N - Z)/2$$

may populate states with isospin  $T_0$  and  $T_0 + 1$ , commonly referred to as  $T_<$  and  $T_>$ , respectively, except in the case of self-conjugate nuclei, where, in the limit of zero momentum transfer (generally applicable to excitation of the GDR with real photons), only states with  $T_> = 1$  can be populated. The states formed by these excitations make up the  $T_<$  and  $T_>$  components of the GDR. According to Fallieros,<sup>31</sup> the energy centroids of these isospin components are split by an amount

$$\Delta E \cong 60(T_0 + 1)/A \text{ MeV}.$$

There is good evidence for this amount of splitting for even- $A$  nuclei near  $A=48$  and elsewhere (Ref. 32; also see, for example, Ref. 33); additional supporting evidence may be sought from the data presented in

this paper.

Since  $^{28}\text{Si}$  is self-conjugate, only  $T_>$  states are populated. Figure 3 [and Fig. 8(a)] therefore represents the neutron decay channel for this GDR. The proton decay channel is very similar,<sup>34</sup> so that it is tempting to consider the observed GDR width of  $\sim 5$  MeV as intrinsic. One then can view the extra width of the GDR for  $^{29}\text{Si}$  [Figs. 4 and 8(b)] as a result of the presence of  $T_<$  strength, separated by

$$\Delta E \cong 60(T_0 + 1)/A \cong 3 \text{ MeV}$$

from the  $T_>$  centroid. This is consistent with the measured width of the GDR for  $^{29}\text{Si}$  of  $\sim 7$  MeV. Similarly, the measured GDR width of  $\sim 8$  MeV for  $^{30}\text{Si}$  [Figs. 7(a) and 8(c)] is consistent with the predicted isospin splitting  $\Delta E \cong 4$  MeV for this nucleus. Moreover, since the photoproton channel has not been considered in this greatly simplified

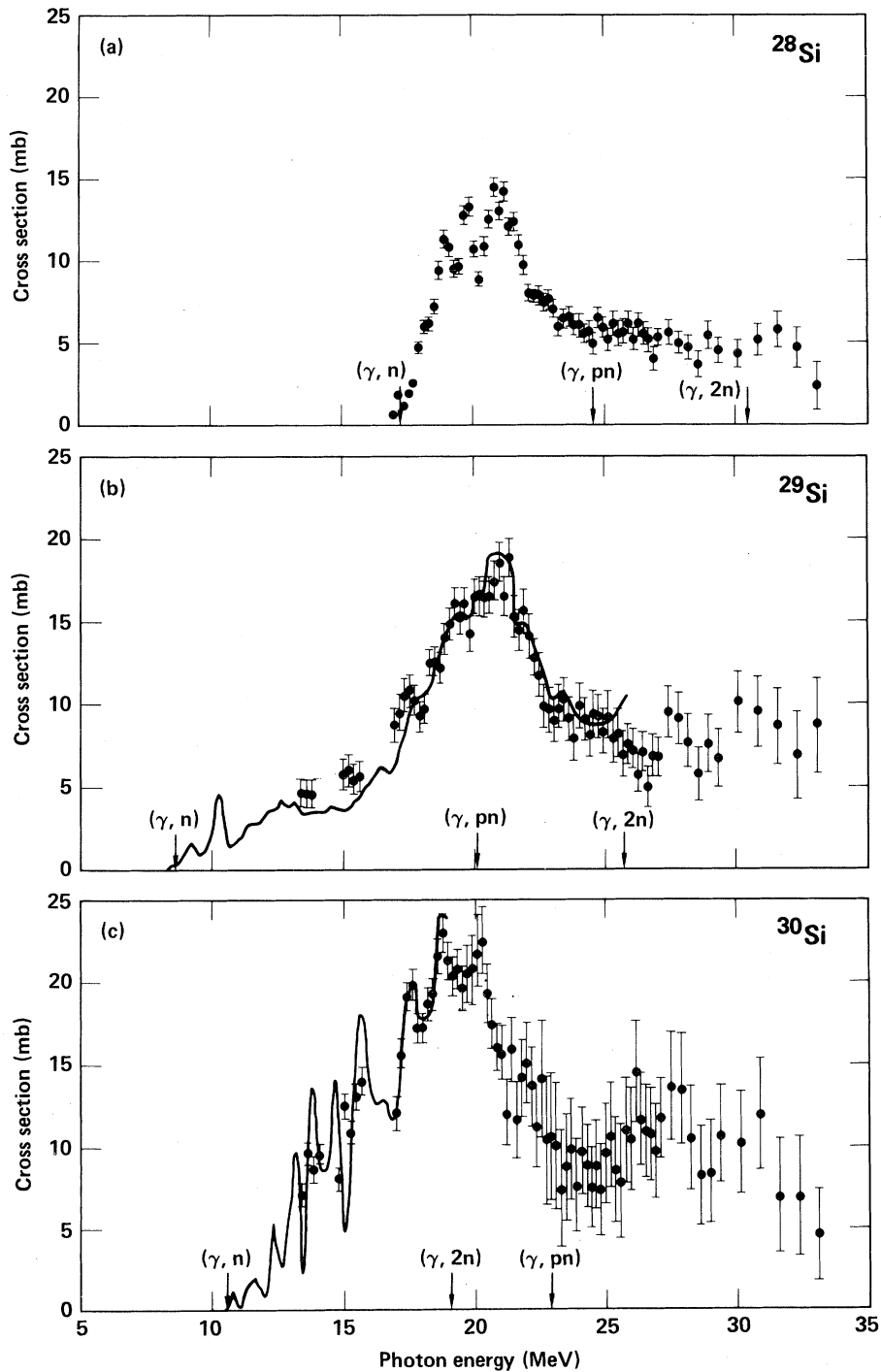


FIG. 8. Total photoneutron cross sections for the silicon isotopes: (a)  $\sigma(\gamma, n_{\text{tot}}) = \sigma(\gamma, 1n)$  for  $^{28}\text{Si}$ ; (b)  $\sigma(\gamma, n_{\text{tot}}) = \sigma(\gamma, 1n)$  for  $^{29}\text{Si}$ ; (c)  $\sigma(\gamma, n_{\text{tot}}) = \sigma[(\gamma, 1n) + (\gamma, 2n)]$  for  $^{30}\text{Si}$ . The data points are the present results; the solid lines represent the recent results from Melbourne [Ref. 6 for  $^{29}\text{Si}$  in part (b) and Ref. 7 for  $^{30}\text{Si}$  in part (c)].

analysis, it is important to note that the inclusion of the  $(\gamma, p)$  cross section might very well lead to somewhat larger measured GDR widths for each case, making the agreement with the predicted values for

$\Delta E$  even better. The shift of the GDR as revealed in the neutron channel, from about 21 to 20 to 19 MeV as one adds neutrons to  $^{28}\text{Si}$ , is also consistent with the predicted isospin splitting of the GDR.

Another important point to note is that on the basis of the weak-coupling model, the photoneutron cross-section strength for  $^{29}\text{Si}$  below about 15 MeV is attributed to excitation of the valence neutron outside the  $^{28}\text{Si}$  core. As such, in this model this strength is of necessity  $T_<$  in nature. Since the isospin nature of this strength can be tested directly by a detailed knowledge of the ground-state photoneutron spectra, such (time-of-flight) measurements are clearly called for.

#### D. Integrated cross sections

In order to facilitate information retrieval for applied purposes and for ease in comparing the present experimental results with theoretical calculations, the integrated cross sections

$$\sigma_{\text{int}} = \int \sigma dE_{\gamma}$$

and their moments

$$\sigma_{-1} = \int \sigma E_{\gamma}^{-1} dE_{\gamma}$$

and

$$\sigma_{-2} = \int \sigma E_{\gamma}^{-2} dE_{\gamma}$$

are shown as running sums versus photon energy in Figs. 9–11. Figure 9 shows these quantities for  $\sigma(\gamma, 1n)$  for  $^{28}\text{Si}$ ; Fig. 10, for  $\sigma(\gamma, 1n)$  for  $^{29}\text{Si}$ ; and Fig. 11 for  $\sigma(\gamma, n_{\text{tot}})$ ,  $\sigma(\gamma, 1n)$ , and  $\sigma(\gamma, 2n)$  for  $^{30}\text{Si}$ . The low-energy  $(\gamma, n)$  cross sections for  $^{29}\text{Si}$  and  $^{30}\text{Si}$  from Refs. 6 and 7 were used for the energy region from the  $(\gamma, n)$  thresholds to 17 MeV. The values for these quantities integrated up to 33.1 MeV (the high-energy limit of the present experiment) are given in Table III. The uncertainties in these quantities should not exceed 10%.

The integrated cross sections for both the photoneutron and photoproton reactions are given in Table IV for the oxygen, magnesium, and silicon isotopes. The values for  $\sigma_{\text{int}}(\gamma, n_{\text{tot}})$  have been obtained largely from monoenergetic-photon measurements, but those for  $\sigma_{\text{int}}(\gamma, p)$  have been obtained (except for  $^{18}\text{O}$ ) from experiments using bremsstrahlung, either by proton detection or by activation, or from  $(e, p)$  measurements. In particular, those measurements which utilized proton detection suffer to a greater or lesser degree from low-energy detection cutoffs and from an imperfect knowledge of the  $(\gamma, p)$  angular distributions, as well as from the usual systematic uncertainties associated with unfolding techniques. We therefore have attempted to attach realistic uncertainties, somewhat larger than those quoted in the references, to several of the values in Table IV [we have done this as well for the relatively old  $\text{Mg}(\gamma, n)$  results of Refs. 2 and 27]. Allowance

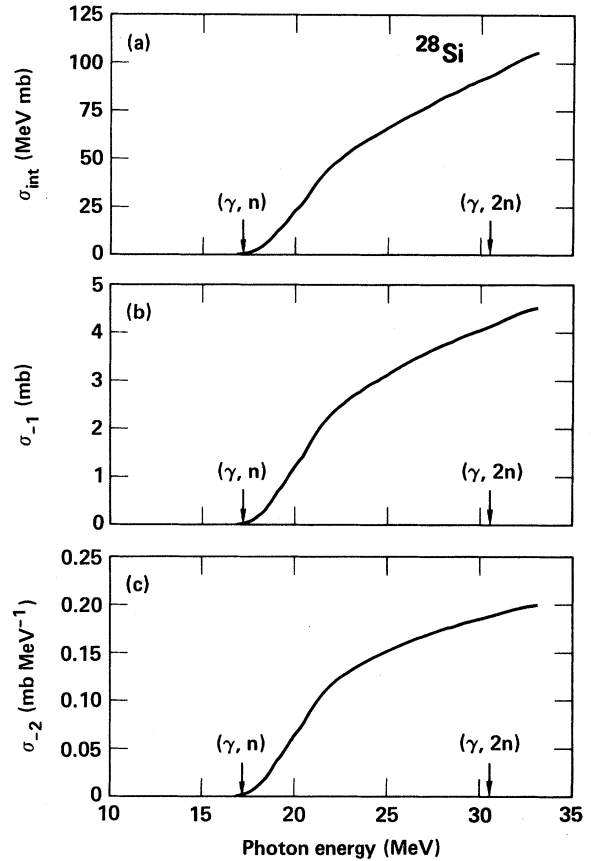


FIG. 9. Integrated photoneutron cross section and its moments for  $^{28}\text{Si}$  as functions of the upper limit of integration:

$$(a) \sigma_{\text{int}} = \int \sigma(E_{\gamma}) dE_{\gamma};$$

$$(b) \sigma_{-1} = \int \sigma(E_{\gamma}) E_{\gamma}^{-1} dE_{\gamma};$$

$$(c) \sigma_{-2} = \int \sigma(E_{\gamma}) E_{\gamma}^{-2} dE_{\gamma}.$$

The integrated cross section or its moments over any desired limits can be obtained from these curves by subtraction.

also has been made for extrapolations from lower energies in several cases. Although the values for  $\sigma_{\text{int}}(\gamma, p)$  for  $^{24}\text{Mg}$ ,  $^{25}\text{Mg}$ , and  $^{28}\text{Si}$  could be contaminated by  $(\gamma, pn)$  events, we judge that such effects are small for these cases.

Values of the sum of  $\sigma_{\text{int}}(\gamma, n_{\text{tot}})$  and  $\sigma_{\text{int}}(\gamma, p)$ , in Thomas-Reiche-Kuhn (TRK) sum-rule units, and for the ratio of  $\sigma_{\text{int}}(\gamma, p)$  and  $\sigma_{\text{int}}(\gamma, n_{\text{tot}})$  are also given in Table IV. It is of interest to compare the values for

$$\sigma_{\text{int}}[(\gamma, n_{\text{tot}}) + (\gamma, p)]$$

for  $^{28}\text{Si}$  with the values for  $\sigma_{\text{int}}(\gamma, \text{tot})$  obtained from

total photon-absorption measurements of  $^{nat}\text{Si}$ . Such a comparison is valid because the contribution of the  $(\gamma, \alpha)$  channel (which is ignored in the former) and the contributions from  $^{29}\text{Si}$  and  $^{30}\text{Si}$  contamination (in the latter) both are small effects. The values for  $\sigma_{\text{int}}(\gamma, \text{tot})$  are 0.79 TRK units (Ref. 21), 0.86 TRK units (Ref. 22), 1.01 TRK units (Ref. 23), and 0.71 TRK units [from a new measurement at Ottawa (Ref. 43), extrapolated slightly from a value of 0.69 TRK units up to 29 MeV]. These values scatter about that for

$$\sigma_{\text{int}}[(\gamma, n_{\text{tot}}) + (\gamma, p)] = 0.79 \pm 0.09$$

TRK units. However, it should be noted that the value from Ref. 23 is  $\sim 30\%$  larger than the sum of the integrated partial cross sections, just as is the case for  $^{16}\text{O}$  when the data for  $\sigma_{\text{int}}(\gamma, \text{tot})$  from Ref. 23 are used (see Ref. 35 for a detailed discussion of the  $^{16}\text{O}$  case).

Although it is clear from Table IV that for the self-conjugate nuclei  $^{16}\text{O}$ ,  $^{24}\text{Mg}$ , and  $^{28}\text{Si}$  the ratio

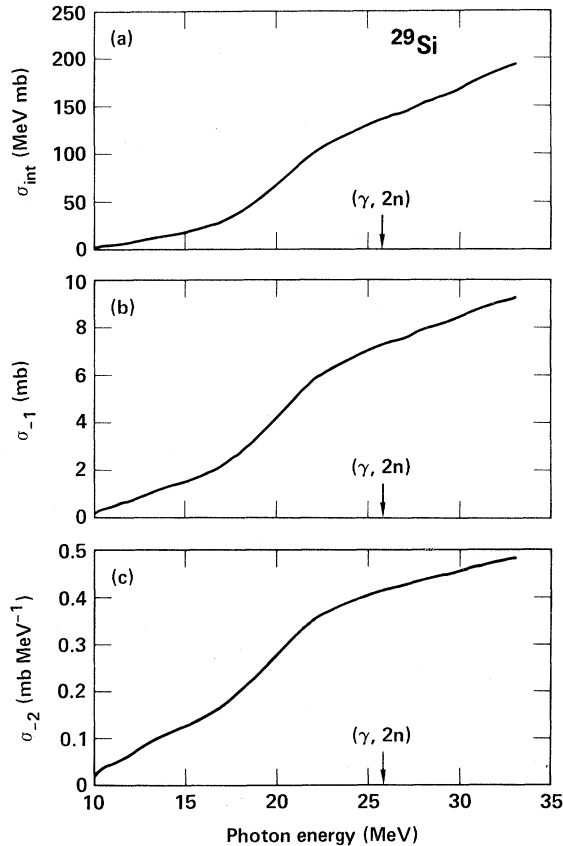


FIG. 10. Integrated photoneutron cross section and its moments for  $^{29}\text{Si}$  as functions of the upper limit of integration: (a)  $\sigma_{\text{int}}$ ; (b)  $\sigma_{-1}$ ; (c)  $\sigma_{-2}$ . Data from Ref. 6 have been used for the energy region below 17 MeV.

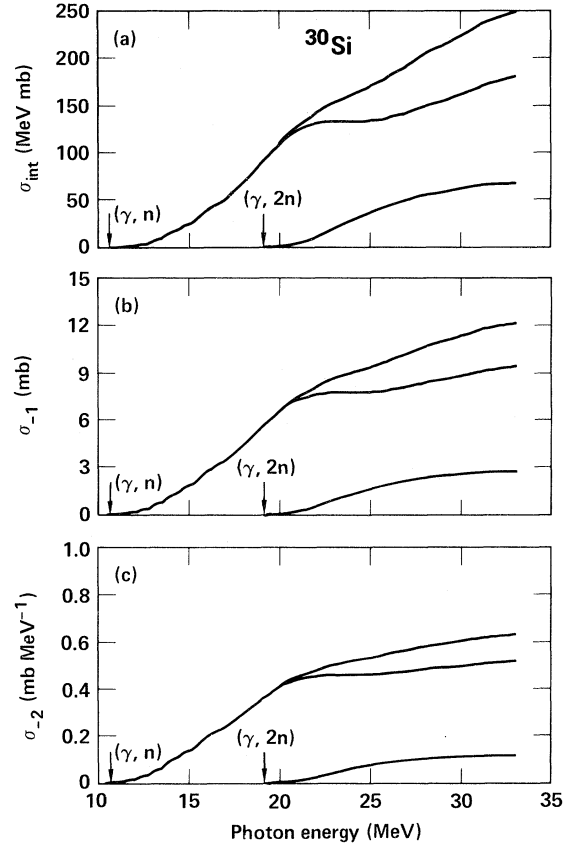


FIG. 11. Integrated photoneutron cross sections and their moments for  $^{30}\text{Si}$  as functions of the upper limit of integration: (a)  $\sigma_{\text{int}}$ ; (b)  $\sigma_{-1}$ ; (c)  $\sigma_{-2}$ . The top curves in each part of the figure are for  $\sigma(\gamma, n_{\text{tot}})$ , the middle curves are for  $\sigma(\gamma, 1n)$ , and the bottom curves are for  $\sigma(\gamma, 2n)$ . Data from Ref. 7 have been used for the energy region below 17 MeV.

TABLE III. Integrated cross sections and their moments.<sup>a,b</sup>

Reaction	$\sigma_{\text{int}}$ (MeV mb)	$\sigma_{-1}$ (mb)	$\sigma_{-2}$ (mb MeV <sup>-1</sup> )
$^{28}\text{Si}(\gamma, 1n)$	105.3	4.52	0.200
$^{29}\text{Si}(\gamma, 1n)$	194.5	9.27	0.482
$^{30}\text{Si}(\gamma, 1n)$	181.2	9.37	0.516
$^{30}\text{Si}(\gamma, 2n)$	67.5	2.72	0.111
$^{30}\text{Si}(\gamma, n_{\text{tot}})$	248.7	12.09	0.627
$^{30}\text{Si}(\gamma, xn)^c$	316.2	14.80	0.738

<sup>a</sup>From threshold to 33.1 MeV.

<sup>b</sup>The values for  $^{29}\text{Si}$  and  $^{30}\text{Si}$  [except for the  $(\gamma, 2n)$  reaction] make use of the data of Refs. 6 and 7 for the energy region from the  $(\gamma, n)$  thresholds up to 17 MeV.

<sup>c</sup> $\sigma(\gamma, xn) = \sigma[(\gamma, 1n) + 2(\gamma, 2n)]$ .

$$R = \sigma_{\text{int}}(\gamma, p) / \sigma_{\text{int}}(\gamma, n_{\text{tot}})$$

is significantly larger than unity, and for the  $4N + 2$  nuclei  $^{18}\text{O}$ ,  $^{26}\text{Mg}$ , and  $^{30}\text{Si}$  that it is significantly smaller than unity, the case of the  $4N + 1$  nuclei in these isotopic series is not so clear: The value of  $R$  for  $^{25}\text{Mg}$  is small and that for  $^{29}\text{Si}$  is large. Unfortunately, there are no data for  $^{17}\text{O}(\gamma, p)$ ; however, for two other  $4N \pm 1$  nuclei,  $^{13}\text{C}$  and  $^{15}\text{N}$ , the values for  $R$  [0.58 (Ref. 3) and 0.78 (Ref. 5), respectively] are less than unity. Thus it would seem that  $^{29}\text{Si}$  is the exceptional case, but whether this is because  $\sigma_{\text{int}}(\gamma, n_{\text{tot}})$  is small (by comparison with  $^{25}\text{Mg}$  but not with  $^{17}\text{O}$ ) or because  $\sigma_{\text{int}}(\gamma, p)$  is large (compared with  $^{25}\text{Mg}$ ) is not clear; a measurement of the  $^{17}\text{O}(\gamma, p)$  reaction might help greatly.

In an attempt to shed further light on this question, we have performed a statistical calculation of  $R$  for  $^{25}\text{Mg}$ ,  $^{26}\text{Mg}$ ,  $^{29}\text{Si}$ , and  $^{30}\text{Si}$  which is based upon the expected decay properties of the  $T_{<}$  and  $T_{>}$  components of the GDR, as was done for the  $1f$ - $2p$ -shell nuclei ( $42 \leq A \leq 54$ ) in Ref. 44 (and reported in Ref. 32). Although (as noted in Sec. IV B) this kind of calculation cannot necessarily be expected to be valid for nuclei as light as these (and certainly would not be expected to hold for the oxygen iso-

topes or for the self-conjugate nuclei  $^{24}\text{Mg}$  and  $^{28}\text{Si}$ ), it is nevertheless suggested by the statistical-like behavior of the partial photoneutron cross sections for  $^{30}\text{Si}$ . For this calculation, both the  $T_{<}$  and  $T_{>}$  absorption widths were set equal to 5 MeV (see Sec. IV C) and the GDR centroid energies were chosen according to the droplet model.<sup>45</sup> The  $(\gamma, \alpha)$  cross sections were set equal to zero because it was found that their inclusion made very little difference to the results. It was found as well that varying the energy and width of the input absorption cross sections and changing the energy-level distributions made little difference; even large changes of these parameters make only small changes to the results for  $R$ . The calculated results are dominated by the location of the particle thresholds, and are reasonable for these cases where the thresholds are low enough so that there are a large number of states available for decay.

The calculated values of  $R$  are 0.35 for  $^{26}\text{Mg}$  and 0.4 for  $^{30}\text{Si}$ , in agreement with the experimental values given in Table IV. The calculated value for  $^{29}\text{Si}$  is 1.8, which is likewise in agreement with experiment. The calculated value for  $^{25}\text{Mg}$ , however, is 1.3, much larger than the experimental value of 0.45; thus perhaps it is  $^{25}\text{Mg}$  that is the exceptional

TABLE IV. Integrated photonuclear cross sections up to 30 MeV.

Nucleus	$\int \sigma(\gamma, n_{\text{tot}}) dE_{\gamma}$		$\int \sigma(\gamma, p) dE_{\gamma}$		Sum TRK units	Ratio $\sigma_{\text{int}}(\gamma, p) / \sigma_{\text{int}}(\gamma, n_{\text{tot}})$
	(MeV mb)	TRK units	(MeV mb)	TRK units		
$^{16}\text{O}$	$55 \pm 3^a$	$0.23 \pm 0.01$	$91 \pm 12^b$	$0.38 \pm 0.05$	$0.61 \pm 0.06$	$1.65 \pm 0.30$
$^{17}\text{O}$	$95 \pm 10^c$	$0.37 \pm 0.04$	not available			
$^{18}\text{O}$	$142 \pm 14^d$	$0.53 \pm 0.05$	$31 \pm 3^d$	$0.12 \pm 0.01$	$0.65 \pm 0.06$	$0.22 \pm 0.04$
$^{24}\text{Mg}$	$57 \pm 9^e$	$0.16 \pm 0.03$	$170_{-40}^{+20 f}$	$0.47_{-0.11}^{+0.06}$	$0.63_{-0.12}^{+0.08}$	$3.0_{-1.2}^{+0.8}$
$^{25}\text{Mg}$	$257 \pm 30^g$	$0.69 \pm 0.08$	$115 \pm 16^h$	$0.31 \pm 0.04$	$0.99 \pm 0.10$	$0.45 \pm 0.12$
$^{26}\text{Mg}$	$254 \pm 30^i$	$0.65 \pm 0.08$	$90 \pm 20^j$	$0.23 \pm 0.05$	$0.89 \pm 0.11$	$0.35 \pm 0.12$
$^{28}\text{Si}$	$91 \pm 9^k$	$0.22 \pm 0.02$	$243 \pm 32^l$	$0.58 \pm 0.08$	$0.79 \pm 0.09$	$2.7 \pm 0.7$
$^{29}\text{Si}$	$168 \pm 17^k$	$0.39 \pm 0.04$	$274 \pm 50^m$	$0.63 \pm 0.11$	$1.02 \pm 0.12$	$1.6 \pm 0.45$
$^{30}\text{Si}$	$235 \pm 23^k$	$0.52 \pm 0.05$	$111 \pm 20^m$	$0.25 \pm 0.04$	$0.77 \pm 0.08$	$0.5 \pm 0.15$

<sup>a</sup>References 11 and 35.

<sup>b</sup>Reference 36; also see Ref. 35.

<sup>c</sup>Reference 4.

<sup>d</sup>Reference 1.

<sup>e</sup>Reference 2, extrapolated from 28.3 MeV.

<sup>f</sup>References 37 and 38.

<sup>g</sup>Reference 27, extrapolated from 28.9 MeV.

<sup>h</sup>Reference 34, extrapolated from 26 MeV.

<sup>i</sup>Reference 2, extrapolated from 28.6 MeV.

<sup>j</sup>Reference 39; more recent data up to 23 MeV from Ref. 40 are in close agreement.

<sup>k</sup>Present work.

<sup>l</sup>Reference 34, extrapolated from 26 MeV; very recent data up to 22.5 MeV from Ref. 41 are in agreement; also see Ref. 42.

<sup>m</sup>Reference 30, extrapolated from 26 MeV.

case. Obviously, more data are needed; in addition to  $^{17}\text{O}(\gamma, p)$ , measurements of the sulfur isotopes might help to clarify the issue.

#### E. The validity of $^{28}\text{Si}$ as a "core" nucleus

It is reasonable that the present results for the silicon isotopes be compared and contrasted with those for the oxygen and magnesium isotopes, as they all share a common  $4N + M$  grouping, with  $N=4, 6,$  and  $7$  and  $M=0, 1,$  and  $2,$  respectively, and with the "base" members all having  $J^\pi=0^+, T=0$  ground states. However, whereas  $^{16}\text{O}$  is a closed-shell nucleus,  $^{28}\text{Si}$  is not; calculations by Wong,<sup>46</sup> for instance, give occupancies of 8.3, 2.2, and 1.5 for the  $d_{5/2}, d_{3/2},$  and  $s_{1/2}$  nucleons outside the  $^{16}\text{O}$  shell, while Rowe<sup>47</sup> calculates 6.7, 2.7, and 2.6 for the same parameters. Wong further gives 9.1, 2.1, and 1.8 occupancy factors for  $^{29}\text{Si}$  and 9.6, 2.3, and 2.1 for  $^{30}\text{Si}$ . Although not without ambiguity, recent experimental electron-scattering data<sup>48</sup> give the distribution of the last neutron in  $^{29}\text{Si}$  to be 0.07, 0.44, and 0.49 in these orbits. Despite the lack of agreement between calculations and experiment, the  $(4N + 1)$  and  $(4N + 2)$  nucleons do not appear to be purely valence neutrons weakly coupled to a  $d_{5/2}$  core.

Nonetheless, very apparent similarities exist between the progressions of the various cross sections for the isotopes of silicon and oxygen. In both cases, the  $(\gamma, n_{\text{tot}})$  cross section of the  $M=0$  member has a structured GDR, the  $M=1$  member has a relatively featureless GDR with a structured pygmy resonance, and the  $M=2$  member has marked structure below the GDR as well as a structured GDR. All have substantial high-energy tails. The integrated cross sections rise rapidly in both cases with increasing  $M$ ;  $\int_{30}^{\infty} \sigma dE$  doubles from  $^{16}\text{O}$  to  $^{18}\text{O}$  and from  $^{28}\text{Si}$  to  $^{30}\text{Si}$ . The magnitude of the cross section in the pygmy-resonance region also increases rapidly with  $M$ , in keeping with the concept of isospin splitting.

A noticeable feature in the  $^{30}\text{Si}(\gamma, n)$  cross section is the sudden dropoff after the opening of the  $(\gamma, 2n)$  channel. As pointed out earlier, this is not seen in  $^{18}\text{O}$ , but because the  $(\gamma, 2n)$  threshold in that nucleus is so low, well below the GDR, the effect might be

masked. Moreover, a similarity between the behavior of the two nuclei may exist in the effect of the  $(\gamma, pn)$  channel. The rise in the  $(\gamma, 1n)$  cross section for  $^{30}\text{Si}$  leading to the hump near 27 MeV is ascribed here to the opening of the  $(\gamma, pn)$  channel at 22.9 MeV; the broad hump in  $^{18}\text{O}$  at 27 MeV may also result from the opening of this channel at 21.8 MeV.

The  $(\gamma, 2n)$  cross section is very large both for  $^{18}\text{O}$  (typically  $\sim 4$  mb) and for  $^{30}\text{Si}$  (up to  $\sim 10$  mb), but very small for both  $^{17}\text{O}$  and  $^{29}\text{Si}$  (less than 1 mb for the former, despite its low threshold, and less than 0.2 mb for the latter). This contrasts with the statistical "chewing away" of the  $(\gamma, n)$  strength by the  $(\gamma, 2n)$  reaction typical of heavier elements [e.g., the zirconium isotopes (Ref. 15)], where this phenomenon sets in with the first neutron outside a closed shell.

Finally, as noted in Sec. IV B, the high-energy rise of  $\bar{E}_n$  for  $^{29}\text{Si}$  is reminiscent of that for  $^{17}\text{O}$  (and  $^{13}\text{C}$ ), probably indicating the presence of  $T <$  strength well above the GDR.

Thus, despite the fact that  $^{16}\text{O}$  is a closed shell and  $^{28}\text{Si}$  is not, there appear to be many similarities in the photoneutron systematics of the oxygen and silicon isotopes. It seems that the  $^{28}\text{Si}$  core is more symmetric and "closed" than theory suggests, or that angular-momentum, energy, and isospin considerations outweigh the openness of its shell structure. Alternatively, one can speculate that an electromagnetic probe, particularly the photon, selects out the  $4N + 1$  and  $4N + 2$  aspects of the shell structure of light nuclei, even in the middle of the  $2s-1d$  shell, and thus highlights nuclear phenomena that are not necessarily representative either of hadron-induced reactions or of open-shell calculations.

#### ACKNOWLEDGMENTS

This work was performed at Lawrence Livermore National Laboratory under the auspices of the U.S. Department of Energy under Contract No. W-7405-ENG-48 and also was supported in part by the Natural Sciences and Engineering Research Council of Canada, the University of Melbourne, and the University of Saskatchewan. We thank Dr. D. D. Faul for his valuable help.

\*Permanent address: Department of Physics, Trent University, Peterborough, Ontario, Canada K9J 7B8.

<sup>1</sup>J. G. Woodworth, K. G. McNeill, J. W. Jury, R. A. Alvarez, B. L. Berman, D. D. Faul, and P. Meyer, Phys. Rev. C **19**, 1667 (1979).

<sup>2</sup>S. C. Fultz, R. A. Alvarez, B. L. Berman, M. A. Kelly, D. R. Lasher, T. W. Phillips, and J. McElhinney, Phys.

Rev. C **4**, 149 (1971).

<sup>3</sup>J. W. Jury, B. L. Berman, D. D. Faul, P. Meyer, K. G. McNeill, and J. G. Woodworth, Phys. Rev. C **19**, 1684 (1979).

<sup>4</sup>J. W. Jury, B. L. Berman, D. D. Faul, P. Meyer, and J. G. Woodworth, Phys. Rev. C **21**, 503 (1980).

<sup>5</sup>J. W. Jury, B. L. Berman, J. G. Woodworth, M. N.

- Thompson, R. E. Pywell, and K. G. McNeill, *Phys. Rev. C* **26**, 777 (1982).
- <sup>6</sup>R. E. Pywell, B. L. Berman, P. Kean, and M. N. Thompson, *Nucl. Phys.* **A369**, 141 (1981).
- <sup>7</sup>G. Odgers, B. L. Berman, R. E. Pywell, and M. N. Thompson, *Nucl. Phys.* **A388**, 445 (1982).
- <sup>8</sup>E. Bramanis, T. K. Deague, R. S. Hicks, R. J. Hughes, E. G. Muirhead, R. H. Sambell, and R. J. J. Stewart, *Nucl. Instrum. Methods* **100**, 59 (1972).
- <sup>9</sup>R. E. Pywell, M. N. Thompson, and B. L. Berman, *Nucl. Instrum. Methods* **178**, 149 (1980).
- <sup>10</sup>J. G. Woodworth, K. G. McNeill, J. W. Jury, R. A. Alvarez, B. L. Berman, D. D. Faul, and P. Meyer, University of California Lawrence Livermore Laboratory Report No. UCRL-77471, 1978 (unpublished).
- <sup>11</sup>B. L. Berman, J. W. Jury, J. G. Woodworth, R. E. Pywell, K. G. McNeill, and M. N. Thompson, *Phys. Rev. C* (in press).
- <sup>12</sup>A. Veyssi re, H. Beil, R. Berg re, P. Carlos, A. Lepr tre, and A. de Miniac, *Nucl. Phys.* **A227**, 513 (1974).
- <sup>13</sup>P. Carlos, H. Beil, R. Berg re, B. L. Berman, A. Lepr tre, and A. Veyssi re, *Nucl. Phys.* **A378**, 317 (1982).
- <sup>14</sup>J. T. Caldwell, R. L. Bramblett, B. L. Berman, R. R. Harvey, and S. C. Fultz, *Phys. Rev. Lett.* **15**, 976 (1965).
- <sup>15</sup>B. L. Berman, J. T. Caldwell, R. R. Harvey, M. A. Kelly, R. L. Bramblett, and S. C. Fultz, *Phys. Rev.* **162**, 1098 (1967).
- <sup>16</sup>B. L. Berman, R. L. Bramblett, J. T. Caldwell, H. S. Davis, M. A. Kelly, and S. C. Fultz, *Phys. Rev.* **177**, 1745 (1969).
- <sup>17</sup>J. T. Caldwell, R. R. Harvey, R. L. Bramblett, and S. C. Fultz, *Phys. Lett.* **6**, 213 (1963).
- <sup>18</sup>B. I. Goryachev, B. S. Ishkhanov, V. G. Shevchenko, and B. A. Yur'ev, *Yad. Fiz.* **7**, 1168 (1968).
- <sup>19</sup>S. Costa, L. Ferrero, L. Pasqualini, F. Ferrero, and C. Manfredotti, *Lett. Nuovo Cimento* **1**, 346 (1969).
- <sup>20</sup>D. V. Webb, E. G. Muirhead, and B. M. Spicer, *Nucl. Phys.* **A159**, 81 (1970).
- <sup>21</sup>J. M. Wyckoff, B. Ziegler, H. W. Koch, and R. Uhlig, *Phys. Rev.* **137**, B576 (1965).
- <sup>22</sup>N. Bezi c, D. Jamnik, G. Kernel, J. Krajnik, and J. Snajder, *Nucl. Phys.* **A117**, 124 (1968).
- <sup>23</sup>J. Ahrens, H. Borchert, K. H. Czoek, H. B. Eppler, H. Gimm, H. Gundrum, M. Kr ning, P. Riehn, G. Sita Ram, A. Zieger, and B. Ziegler, *Nucl. Phys.* **A251**, 479 (1975).
- <sup>24</sup>K. Shoda, K. Abe, T. Ishizuka, N. Kawamura, and M. Kimura, *J. Phys. Soc. Jpn.* **17**, 735 (1962).
- <sup>25</sup>C.-P. Wu, F. W. K. Firk, and T. W. Phillips, *Nucl. Phys.* **A147**, 19 (1970).
- <sup>26</sup>P. P. Singh, R. E. Segel, L. Meyer-Sch tzmeister, S. S. Hanna, and R. G. Allas, *Nucl. Phys.* **65**, 577 (1965).
- <sup>27</sup>R. A. Alvarez, B. L. Berman, D. R. Lasher, T. W. Phillips, and S. C. Fultz, *Phys. Rev. C* **4**, 1673 (1971).
- <sup>28</sup>S. T. Lim, M. D. Hasinoff, D. F. Measday, T. J. Mulligan, and K. Ebisawa, *Nucl. Phys.* (to be published).
- <sup>29</sup>B. L. Berman and S. C. Fultz, *Rev. Mod. Phys.* **47**, 713 (1975).
- <sup>30</sup>D. Zubanov, R. A. Sutton, and M. N. Thompson (unpublished).
- <sup>31</sup>S. Fallieros, in *Proceedings of the International Conference on Photonuclear Reactions and Applications*, edited by B. L. Berman (Lawrence Livermore Laboratory, Livermore, 1973), p. 401; also see S. Fallieros and B. Goulard, *Nucl. Phys.* **A147**, 593 (1970), and earlier references therein.
- <sup>32</sup>M. N. Thompson, *Lecture Notes in Physics, Nuclear Interactions*, edited by B. A. Robson (Springer, Berlin, 1978), Vol. 92, p. 208.
- <sup>33</sup>P. Paul, see Ref. 31, p. 407.
- <sup>34</sup>R. A. Sutton, M. N. Thompson, M. Hirooka, T. Tanaka, and K. Shoda, Laboratory of Nuclear Science, Tohoku University Research Report 1982, Vol. 15, p. 42.
- <sup>35</sup>B. L. Berman, R. Berg re, and P. Carlos, *Phys. Rev. C* **26**, 304 (1982), and references therein.
- <sup>36</sup>E. G. Fuller, private communication.
- <sup>37</sup>B. S. Ishkhanov, I. M. Kapitonov, V. G. Shevchenko, and B. A. Yur'ev, *Izv. Akad. Nauk SSSR, Ser. Fiz.* **30**, 378 (1966) [*Bull. Acad. Sci. USSR, Phys. Ser.* **30**, 383 (1966)].
- <sup>38</sup>V. V. Varlamov, B. S. Ishkhanov, I. M. Kapitonov, Yu. I. Prokopchuk, and V. I. Shvedunov, *Yad. Fiz.* **30**, 1185 (1979) [*Sov. J. Nucl. Phys.* **30**, 617 (1979)].
- <sup>39</sup>D. W. Anderson, R. F. Petry, and H. J. Fischbeck, *Phys. Rev. C* **9**, 1919 (1974).
- <sup>40</sup>K. Wienhard, K. Bangert, U. E. P. Berg, G. Junghans, R. Stock, and H. Wolf, *Nucl. Phys.* **A280**, 109 (1977).
- <sup>41</sup>R. L. Gulbranson, L. S. Cardman, A. Doron, A. Erell, K. R. Lindgren, and A. I. Yavin, University of Illinois Report ILL-(NU)-81-55, 1982.
- <sup>42</sup>V. V. Varlamov, B. S. Ishkhanov, I. M. Kapitonov, A. N. Panov, and V. I. Shvedunov, *Izv. Akad. Nauk SSSR, Ser. Fiz.* **43**, 186 (1979) [*Bull. Acad. Sci. USSR, Phys. Ser.* **43**, 157 (1979)].
- <sup>43</sup>N. K. Sherman and W. F. Davidson, private communication.
- <sup>44</sup>R. E. Pywell, Ph.D. thesis, University of Melbourne, 1980 (unpublished).
- <sup>45</sup>W. D. Myers, W. J. Swiatecki, T. Kodama, L. J. El-Jaick, and E. R. Hilf, *Phys. Rev. C* **15**, 2032 (1977).
- <sup>46</sup>S. S. M. Wong, private communication.
- <sup>47</sup>D. J. Rowe, private communication.
- <sup>48</sup>H. Miessen, Ph.D. thesis, University of Mainz, 1982 (unpublished); H. Miessen, G. L hrs, H. Rothhaas, W. Bertozzi, S. Kowalski, C. F. Williamson, R. S. Hicks, R. A. Lindgren, G. A. Peterson, and B. L. Berman, in *Proceedings of the Ninth International Conference on High Energy Physics and Nuclear Structure, Versailles, 1981*, edited by P. Catillon, P. Radvanyi, and M. Porneuf (North-Holland, Amsterdam, 1982), p. 225.